Metadata of the article that will be visualized in OnlineFirst

Please note: Images will appear in color online but will be printed in black and white.

1	Article Title	**Molecular dynamics simulations of strain-controlled fatigue behaviour of amorphous polyethylene**	
2	Article Sub- Title		
3	Article Copyright - Year	**Springer Science+Business Media Dordrecht 2014 (This will be the copyright line in the final PDF)**	
4	Journal Name	Journal of Polymer Research	
5	Corresponding Author	Family Name	**Sahputra**
6		Particle	
7		Given Name	**I. H.**
8		Suffix	
9		Organization	Norwegian University of Science and Technology – NTNU
10		Division	Engineering Design and Materials Department
11		Address	Trondheim, Norway
12		e-mail	iwan.h.sahputra@ntnu.no
13	Author	Family Name	**Echtermeyer**
14		Particle	
15		Given Name	**A. T.**
16		Suffix	
17		Organization	Norwegian University of Science and Technology – NTNU
18		Division	Engineering Design and Materials Department
19		Address	Trondheim, Norway
20		e-mail	
21	Schedule	Received	22 May 2014
22		Revised	
23		Accepted	30 September 2014
24	Abstract		
25	Keywords separated by ' - '	Strain-controlled fatigue - Molecular dynamics - Polyethylene - R-ratio - Mean strain	
26	Foot note information		

J Polym Res (2014) 21:577
DOI 10.1007/s10965-014-0577-2

ORIGINAL PAPER

Molecular dynamics simulations of strain-controlled fatigue behaviour of amorphous polyethylene

I. H. Sahputra · A. T. Echtermeyer

Received: 22 May 2014 / Accepted: 30 September 2014

Abstract Fatigue of amorphous polyethylene under low strain was simulated using molecular dynamics. The united atom approach and the Dreiding force field were chosen to describe the interaction between monomers. Molecular dynamics simulations resembling strain-controlled loading fatigue tests in tension-tension mode were performed to study the effect of the R-ratio and mean strain on the mechanical responses. Laboratory fatigue experiments in strain/displacement control were performed at room temperature, and the results were compared to the simulation results. The simulations are able to produce qualitatively similar behaviour to the experimental results, for instance, mean stress relaxation, hysteresis loops in the stress–strain curve, and change in the cyclic modulus. They also show that stress relaxation is enhanced by cyclic loading. The simulations show that cyclic loading changes the total potential energies of the system, especially the van der Waals potential. The changes in the van der Waals potential energy contribute significantly to the increasing of the stiffness of the system. Some changes in dihedral angles with lower energy configurations are observed; however, bond distances and angles do not change significantly. The chains tend to unfold slightly along the loading axis as the fatigue loading progresses.

Keywords Strain-controlled fatigue · Molecular dynamics · Polyethylene · R-ratio · Mean strain

Introduction

Long-term properties of polymers are critical in many applications. Fatigue, stress rupture, stress relaxation, and creep need to be considered. Usually, the effect of cyclic loads and static loads is treated independently. But in many cases they actually happen simultaneously. This paper investigates fatigue under strain control, a situation that would, for example, be experienced by polymeric liners within a composite pressure vessel. The liner will follow the movements of the skin of the pressure vessel when the vessel is pressurized. Stresses in the liner will relax when the pressure is constant. If the pressure vessel sees many pressure cycles, cyclic fatigue loading will also become important.

Analysing the long-term behaviour of liners or polymers in general in such conditions is typically done by a fatigue analysis using an SN approach [1, 2] or, in some cases, fracture mechanics [1, 3]. Creep and stress relaxation are treated separately using viscoelasticity theory. Many assumptions need to be made when performing the calculations. The approach seems to work satisfactorily in engineering praxis, but a better understanding would be beneficial to improve predictions and to combine the effect of cyclic fatigue and static loads.

Molecular dynamics (MD) can model material behaviour based on first principles using atomic (or molecular) potentials. Polymer modelling that is based on more details of chemical structures and fundamental physical science will improve the understanding of the relations between particular properties and molecular structure [4–9]. The increasing use of polymers in nanomaterial applications also requires a deeper knowledge of the atomistic and molecular scales. This paper explores how MD can be used to model effects of cyclic fatigue and stress relaxation. MD calculations require enormous computer power. Even with a supercomputer only a few short polymer chains can be modelled, and simulated test rates are very high compared to laboratory experiments. But even with these limitations some principle response of polymers can be explored.

Some studies have shown that MD is able to predict mechanical properties of polymers deformed at a particular constant strain rate, such as Young's modulus, yield stress, and Poisson's ratio [10–14]. But only few studies of fatigue

I. H. Sahputra (✉) · A. T. Echtermeyer
Engineering Design and Materials Department, Norwegian University of Science and Technology – NTNU, Trondheim, Norway
e-mail: iwan.h.sahputra@ntnu.no

behaviour of polymers using MD are found compared to those for other materials. (Note: in this paper the word "experiment" is always related to physical tests in the laboratory, while the word "simulation" is related to calculated/modelled behaviour).

Yashiro et al. [15] investigated the effect of loading condition and chain length on the behaviour of polyethylene under cyclic loading. Their main finding was the leaf-like hysteresis analogous to experimental results both in stress- and strain-controlled loading, although there was a huge discrepancy in the strain rates. They suggested that short chains may bring the reduction of stiffness and increase of plastic flow deformation. Li et al. [16] studied the thermo-mechanical response of thermosetting polymers, focussing on strain accumulation and energy dissipation. They found that a uniaxial stress condition with zero lateral stress led to the highest rate of strain accumulation compared to purely deviatoric shear stress and uniformly volumetric (hydrostatic) stress. This condition also caused the highest degree of energy dissipation as shown by the highest rise in temperature, calculated assuming an adiabatic condition.

Several laboratory experimental studies have been conducted to show the effect of various loading conditions, such as strain ratio and mean strain, on the strain-controlled fatigue behaviour of polymers [17–21]. This study will investigate to what extent the effect of R-ratio and mean strain on the fatigue behaviour of polymers can be simulated using the MD approach. Considering that the current computing power is not sufficient to model many or long polymer chains subjected to long-term dynamic loading, a fairly simple and small model will be built in this study. Polyethylene is chosen to be modelled, because it has a simple structure and it is used in many applications.

The focus of this study will be on the stress-time responses and stress–strain responses of strain-controlled fatigue. A qualitative comparison of simulations and experiments will be done to evaluate the accuracy of the simulations. The evolution of potential energies and polymer chain structural geometries will be presented and discussed. This effort shall lead to an increased fundamental understanding of polymer behaviour under fatigue on the molecular level.

Model, simulations, and experiments

The united atom approach was chosen to model the PE system. This approach simplifies each group of CH_2 monomers as single monomer particles, e.g. [12–14]. The Dreiding force field [22] was chosen to describe the interactions between monomers. In Dreiding, the potential energy for a molecule consists of the combination of bonded interactions (bond stretch, bond angle bend, and dihedral angle torsion) and a non-bonded interaction (van der Waals, which is represented by the Lennard-Jones potential). The functional forms and parameters [13, 14] of the Dreiding force field are given in Table 1.

The initial PE chain structure was generated using a Monte Carlo self-avoiding random walk algorithm [13, 14]. The basic idea of this method is that each monomer is placed on each site of the face-centered cubic (fcc) lattice with a lattice constant of 1.53 Å. The initial position is randomly selected and the next atom is placed according to the probability for each possible bond angle direction and the density of unoccupied neighbour sites. The structure contains ten chains and each chain consists of 10,000 monomers. It is a very small sample compared to real PE, which consists of a large number of chains and a range of different lengths. A molecular dynamics program designed for parallel computers, LAMMPS [23], was used to simulate the deformation process. All the simulations were performed on the supercomputer system at NTNU.

The initial conditions of the simulation were obtained in a sequence of steps. Initial velocities were assigned to the atoms by randomly selecting from a uniform distribution at a temperature of 500 K. Before performing the dynamic strain cycling simulation, first the Langevin thermostat was applied on the initial structure for 10 ps at 500 K. This thermostat was used within NVE (number of particles, volume, energy) ensembles to perform a Brownian dynamics simulation of a molten polymer. The system was then equilibrated at NPT (number of particles, pressure, temperature) ensembles for 25 ps at 500 K and then cooled to the desired temperature of simulation (300 K) in a step-wise manner for 25 ps. Finally the system once again was equilibrated for 25 ps at the desired deformation temperature.

The NPT ensembles were done using a Nose-Hoover thermostat and barostat [24–26] coupled to the atom velocities and simulation box dimensions. The time integration of the motion equations was done using the time-reversible measure-preserving Verlet and rRESPA integrators [27]. Periodic boundary conditions were applied to all directions of the simulation box.

During the simulated sample preparation processes, pressure and stress were monitored to characterize whether equilibration was satisfied. In the final equilibration stage, all the potential energies (bond, angle, dihedral, and van der Waals) and polymer chain geometries were also monitored to check if the final equilibrium was reached and if the sample was ready to be deformed. Figure 1 shows the polymer chain geometries after the final equilibration stage at 300 K. The mean value of bond length is 1.53 Å with a standard deviation of 0.03 Å, while the mean value of bond angle is 109.30° with a standard deviation of 4.07°.

The glass transition temperature (Tg), indicating the transition between the glassy state to the rubbery state, is an important characteristic of polymers. The glass transition

Table 1 Functional forms and parameters for molecular potential energy

Interaction	Functional form	Parameters
Bond stretch	$V_b=k_b(r_b-r_o)^2$	k_b = 350 kcal/mol r_b = bond length r_o = equilibrium bond length, 1.53 Å
Bond angle	$V_a=k_a(\theta_a-\theta_b)^2$	k_a = 60 kcal/mol θ_a = bond angle θ_b = equilibrium bond angle = 109.5°
Dihedral angle torsion	$V_d = \sum_{n=1}^{4} k_n \cos^{n-1}\phi_d$	K_1 = 1.73 kcal/mol, K_2 = −4.49 kcal/mol K_3 = 0.776 kcal/mol, K_4 = 6.99 kcal/mol ϕ_d = dihedral angle
van der Waals	$V_{ij} = 4\varepsilon\left[\left(\frac{\sigma_{ij}}{r_{ij}}\right)^{12}-\left(\frac{\sigma_{ij}}{r_{ij}}\right)^{6}\right]$ for $r<r_c$	ε_{lj} = 0.112 kcal/mol, σ_{lj} = 4.01 Å r_c = 10 Å

temperature in this study was determined from the change in slope of the volume vs. temperature curve. Figure 2 shows a plot of the volume of the sample as a function of temperature. The intersection of the two trend lines of the data shows that the estimation of the glass transition temperature of the sample is around 260–280 K. This is close to the experimentally measured value of 250 K [28].

The equilibrium in a random amorphous system is not defined in a unique way for the molecular structure. A good way to check whether a reasonable equilibrium was reached during the initial system simulation is to compare the characteristic ratio *C* with experimental data [29]:

$$C = \langle r^2 \rangle / nl^2 \quad (1)$$

where $\langle r^2 \rangle$ is the average end-to-end distance of the chain, n is the number of chains, and l is bond length.

The *C* of polyethylene is estimated from direct experimental intrinsic viscosity measurements to be 7.10, 6.99, and 6.80 at temperatures of 127.5 °C, 142.2 °C, and 163.9 °C, respectively [30]. The simulated sample of this study, after equilibrating at a temperature of 500 K (=227 °C) has a characteristic ratio of 5.3. This indicates that the simulation sample is composed of more tightly coiled chains compared to the real polyethylene. The accuracy of the stress–strain response of glassy polymers with MD simulations depends on the characteristic ratio [29]. However, the accuracy of C is especially important for the stress–strain response after the yield stress and for the slope of the rehardening part, typically above 20 % of strain. The initial low strain is not influenced much by the value of C. As in this study the mean strains were set 2 %, 5 %, and 10 % the model is considered adequate for the objective of this study.

Fatigue loading was simulated by sinusoidally oscillating the NPT ensemble's length in the x-direction, L(t), using the following equation:

$$L(t) = L0 + A\sin(2p.t/T) \quad (2)$$

Where L0 is the initial system length, A is the amplitude, t is the time, and T is the period. The other two directions were kept at zero pressure, allowing the simulation box to contract sideways. Before applying a sinusoidal strain loading, the sample was deformed to the initial strain with a constant strain rate, as shown in Fig. 3. The R-ratios were 0.48, 0.67, and 0.9, and the mean strains were 10 %, 5 %, and 2 %, where:

$$R-ratio = \text{minimum strain}/\text{maximum strain} \quad (3)$$

$$\text{Mean strain} = (\text{maximum strain} + \text{minimum strain})/2 \quad (4)$$

Note that R=0.9 has a high mean strain and low amplitude, getting close to stress relaxation.

This simulation resembles the strain-controlled fatigue test in tension-tension mode. The frequency of the sinusoidal waveform displacement was 10^{12} Hz. The maximum strain rate at the steepest slope of the sinusoidal loading varied from 43.4×10^9 s^{-1} to 8.7×10^9 s^{-1} depending on the R-Ratio.

Similar strain-controlled fatigue experiments on PE samples were also performed in the laboratory at room temperature in order to compare the simulation results. The comparison is not ideal, because the experimental HDPE has a high crystallinity content, while the simulation was done for amorphous PE. For practical reasons the test frequency had to be much lower than in the simulations. Sinusoidal displacement was applied at a frequency of 2 Hz, mean strains were 2 % and 5 %, and R-ratios were 0.48, 0.67, and 0.75. The test samples were cut from a PE sheet (Polystone M-Black-AST, manufactured by Rochling Engineering Plastic). It is a high-density polyethylene (HDPE) which has a molecular weight of 9.2×10^6 g/mol and a density of 0.945 g/cm^3. The shape and dimension of the samples were

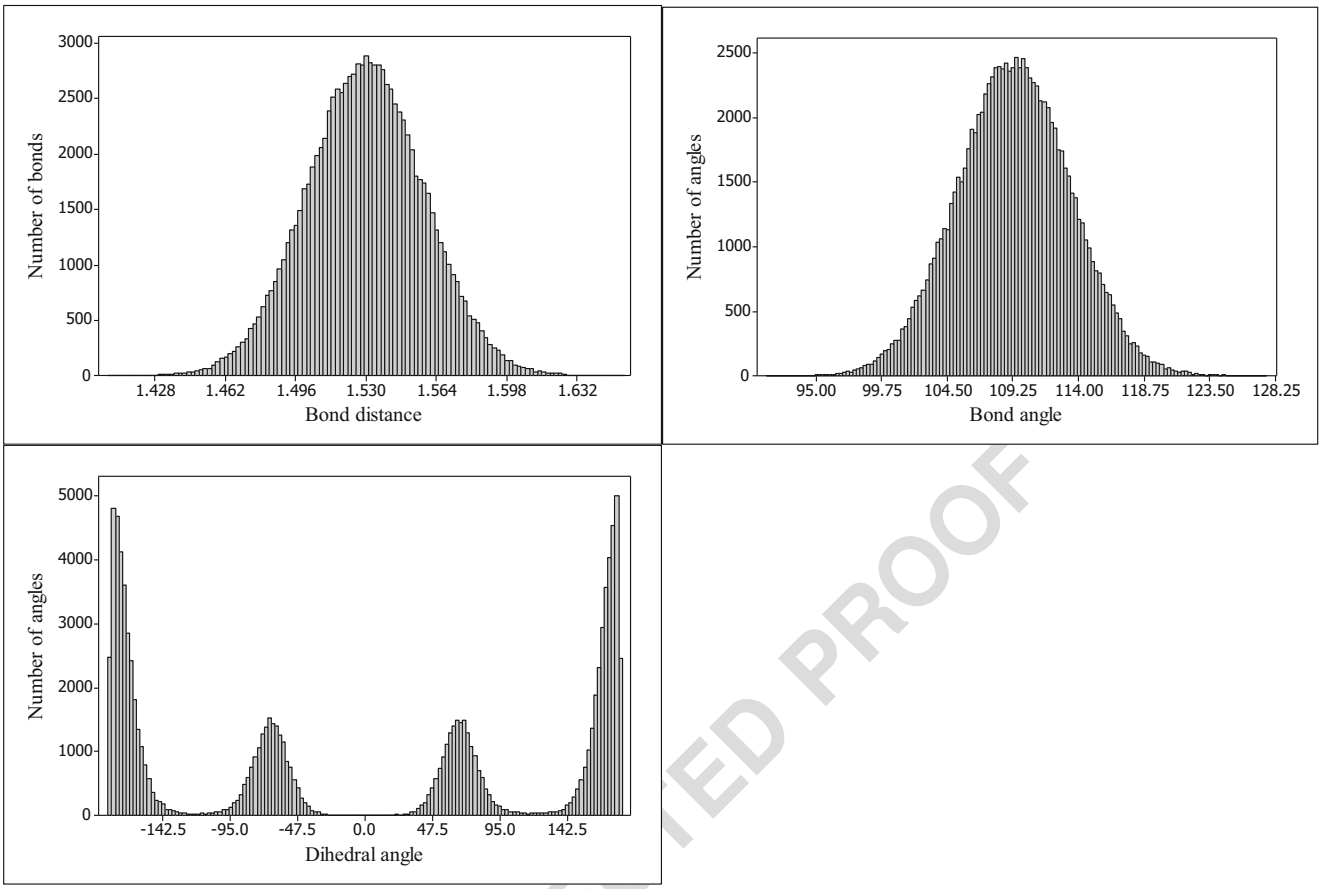

Fig. 1 Distribution of polymer chain geometries after the final equilibration stage

according to ISO 527–2:2012 type 1B standard and the thickness was 3 mm. Loads were recorded by a computerized data acquisition system. Stresses were calculated as load of initial cross-sectional area (engineering stresses). The initial measurements from 0 to 10 s were not used, because the test machine had not reached the steady state strain amplitude yet.

Results and discussions

Figure 4 shows the stress response to the first two cycles of sinusoidal loading in the MD simulation with an R-ratio of 0.48 and mean strain of 2 %. Both stress (σ) and strain (ε) are normalized to the stress and strain at time zero of the fatigue cycles ($\sigma_{(t)}$ normalized=$\sigma_{(t)}/\sigma_{(t=0)}$ and $\varepsilon_{(t)}$ normalized=$\varepsilon_{(t)}$/

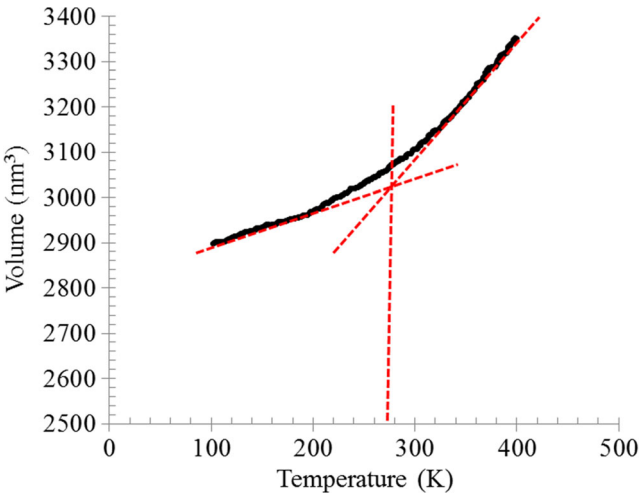

Fig. 2 Glass transition temperature (Tg) of the simulation model

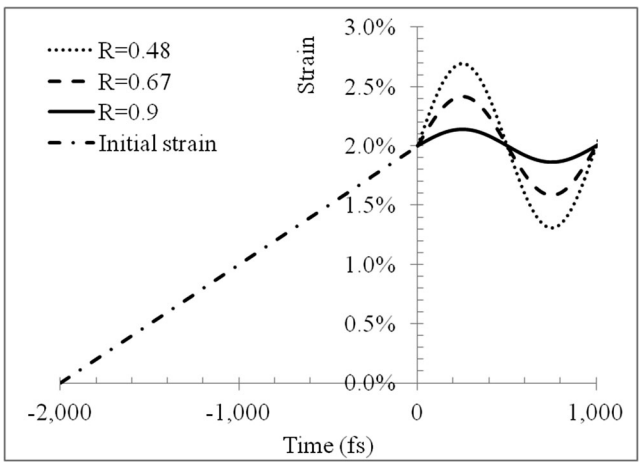

Fig. 3 Initial and sinusoidal strain loading of the simulations (mean strain, 2 %)

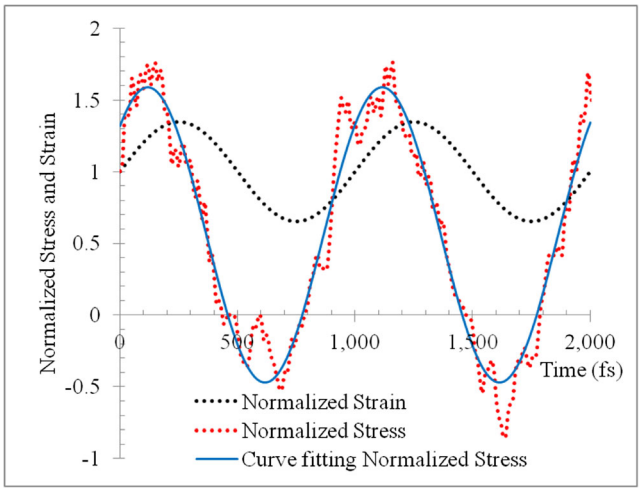

Fig. 4 Alternating stress response to the sinusoidal strain input in the simulation

$\varepsilon_{(t=0)}$). The initial time to reach the mean strain before fatigue cycling starts is not considered here. The jumps or vibrations in the simulated stress are due to the stepwise calculations of the simulation and modelling uncertainties. As shown in Fig. 4, by applying the Trust-Region fitting method [31, 32] for the first 2,000 ps of the simulation, we get the following:

$$\varepsilon_{(t)}\text{normalized} = 1 + 0.35\sin\left(6.3 \times 10^{-3}t\right) \quad (5)$$

$$\sigma_{(t)}\text{normalized} = 0.56 + 1.03\sin\left(6.3 \times 10^{-3}t + 0.83\right) \quad (6)$$

The normalized strain lags behind the normalized stress by a phase angle similar to the typical response of viscoelastic material. For a linear viscoelastic material, the stress response to an oscillatory sinusoidal shear strain is also sinusoidal, but is out of phase with the strain.

In the following sub-sections the effect of R-ratio and mean strain will be discussed. The last sub-section will discuss the evolution of potential energy and structural geometry of the polymer chains during simulations.

Effect of R-ratio on the mechanical behaviour

Figure 5 shows the difference in cyclic stress responses produced by the simulations and experiments using various R-ratios, but the same mean strains. The experimental mean stresses for the first 20 cycles were omitted from the figures because the machine had not reached the steady state strain amplitude as mentioned in the previous section. A trend of decreasing mean stress (stress relaxation) along the loading is observed. As expected, increasing the R-ratio reduces the stress range/amplitude as shown in Fig. 5a. Figure 5b /Q1

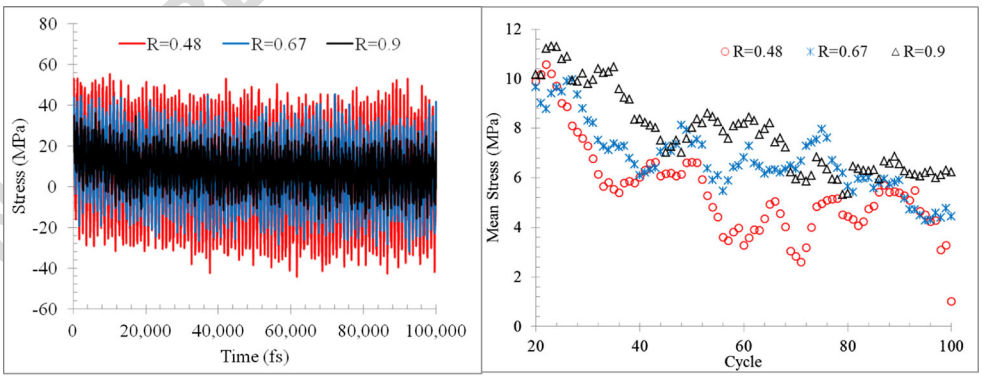

(a) Calculated stress response..

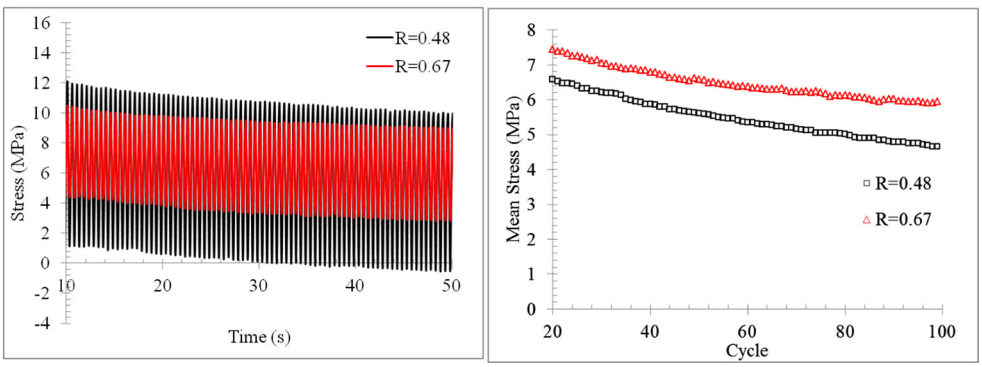

(b) Experimental stress response.

Fig. 5 Stress responses to the various R-ratios. a Calculated stress response; b experimental stress response

presents the stress responses of the laboratory experiments with R-ratios 0.48 and 0.67. The stresses show similar behaviour as in the simulations, the mean stress relaxation occurs and reaches a stable level in a short period of cycles.

Different magnitudes of stresses between the simulations and experiments are found because of the discrepancy of the cyclic frequency and molecular properties, for instance molecular weight, degree of crystallinity, and molecular orientation [13, 33–35]. Future work is planned to model the crystalline part as well, and with increasing computer power, simulations at lower frequency may also become possible. It is nevertheless interesting to see similar trends despite the limitations.

Although the effect is small, simulations and experiments show that cyclic fatigue loading accelerates the effect of stress relaxation.

Stress–strain curves of the simulations and experiments are presented in Fig. 6. The three simulation results show hysteresis loops in the stress–strain curves. The hysteresis loops move downward (lower stresses) as cycling progresses from cycles 1–5 to cycles 95–100. Increasing the R-ratio increases the downward shift of the hysteresis loops. Meanwhile, the enclosed area of the hysteresis loop decreases with increasing R-ratio.

Figure 6e presents the stress–strain curves of the experiments with R-ratios 0.48 and 0.67, respectively. The hysteresis loops move downward with the cycles as seen in the

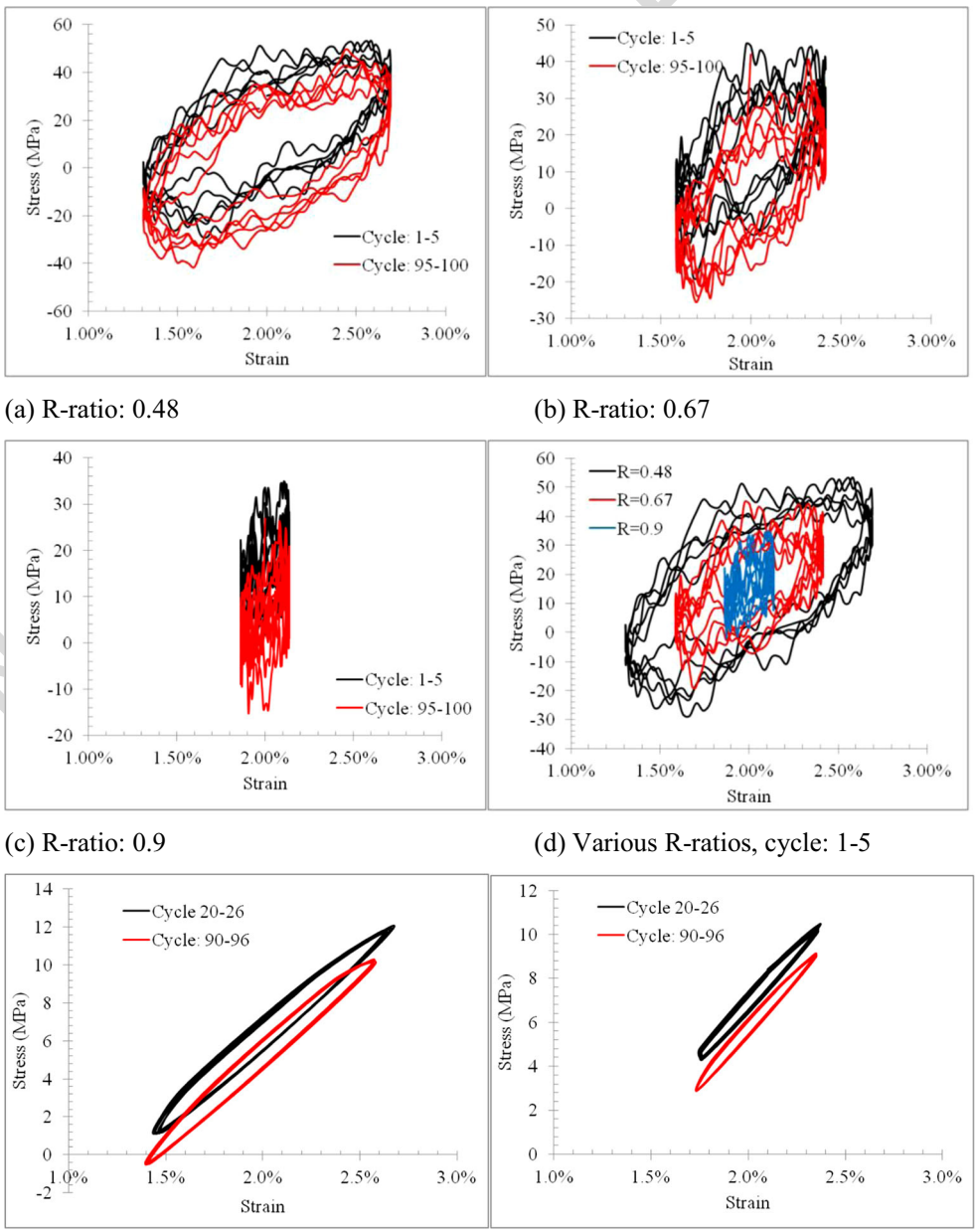

(a) R-ratio: 0.48

(b) R-ratio: 0.67

(c) R-ratio: 0.9

(d) Various R-ratios, cycle: 1-5

(e) Experimental results for. R-ratios: 0.48 (left) and R-ratio: 0.67 (right)

Fig. 6 Stress–strain response at various R-ratios. a R-ratio, 0.48; b R-ratio, 0.67; c R-ratio, 0.9; d various R-ratios, cycles 1-5; e experimental results for R-ratios 0.48 (left) and 0.67 (right)

t2.1 **Table 2** Cyclic modulus of the MD simulations and experiments with various R-ratios

t2.2 R-ratio	Simulations (GPa)		Experiments (GPa)	
t2.3	Cycles: 1–2	Cycles: 99–100	Cycles: 20–26	Cycles: 90–96
t2.4 0.48	3.01	3.42	0.88	0.91
t2.5 0.67	3.11	3.62	0.96	0.98
t2.6 0.9	3.74	4.00	*NA*	*NA*

NA not available

experimental results similar to those of simulations. This indicates that the MD simulation is able to show an increase in thermodynamically irreversible damage during cyclic loading linked to an increase in stiffness similar to the experimental results.

The cyclic modulus for each cycle is defined as the slope of the stress–strain curve for each cycle, corresponding to the secant modulus in monotonic loading [36]. Table 2 shows the calculated averaged cyclic modulus for simulations and experiments with various R-ratios. Both simulations and experiments show that increasing R-ratio increases the cyclic modulus. The cyclic modulus also increases along with the cycles. The difference in the magnitude of the modulus between simulations and experiments is related to the discrepancy of the cyclic frequency and molecular properties, as previously discussed.

Effect of mean strain on the mechanical behaviour

The effect of the mean strain-to-stress response is shown in Fig. 7. Higher mean strain obviously increases the mean stress level. This is because below the yield point, the stress is in a close linear relation to the strain and this study is limited to low rates of strain, i.e., below yield. The experimental results in Fig. 6 verify that the simulations are able to produce qualitatively similar trends of various mean strain effect on the stress responses.

Stress–strain curves of the different mean strain values are presented in Fig. 8. Again, the experimental results confirm that the simulations are able to produce quantitatively the effect of mean strain effect on the stress–strain curves. Increasing mean strain increases the amount of downward shift of the hysteresis loops, as seen both in experiments and simulations.

Table 3 shows the effect of the mean strain on the cyclic modulus. Increasing mean strain reduces the cyclic modulus as shown by both simulations and experiments. The cyclic modulus is also increasing along with the cycles. The modulus of the simulation with 10 % mean strain is higher than that of 5 % mean strain at cycles 99–100. The increase is probably due to an orientation of the polymer chains in the load direction resulting in a strain hardening effect. The other possible reason is the limitation of the model to simulate high strain behaviour due to the lower characteristic ratio, C, compared to the real polyethylene. The difference in the magnitude of the modulus between simulations and experiments is again related to the discrepancy of the cyclic frequency and molecular properties, as previously discussed.

Potential energy and chain structure evolution

The effect of increasing modulus due to fatigue has been known from laboratory experiments. A unique feature of MD is the possibility to investigate changes of molecular properties in the polymer related to this effect. The polymer chains get deformed and move against each other from the applied strains or loads. These deformations change the potential energy of the system.

Figure 9 presents the evolution in the total potential energy and the normalized total potential energy, $V(t)/V_{eq}$, of the polymer system in the simulation using a mean strain of 2 % and an R-ratio of 0.48. V_{eq} is the potential energy after the equilibrium steps, before applying the initial mean strain. V(t) is the potential energy at any time after applying the sinusoidal displacement. The polymer chains receive energy from the work done by the sinusoidal displacement.

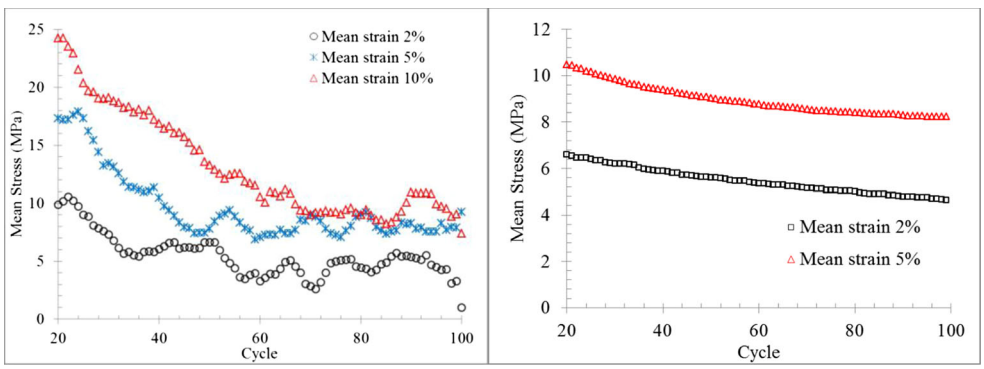

Fig. 7 Mean stress responses from MD simulations and experiments

(a) MD simulations (b) Laboratory experiments

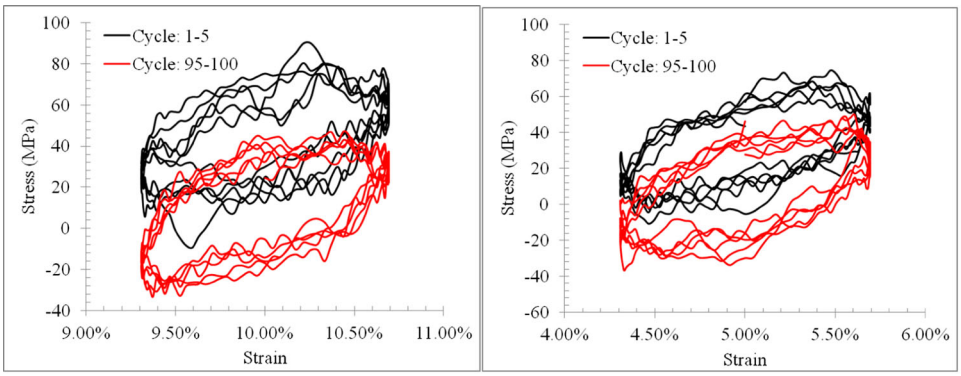

(a) Mean strain: 10%, R-ratio: 0.87 (b) Mean strain: 5%, R-ratio: 0.75

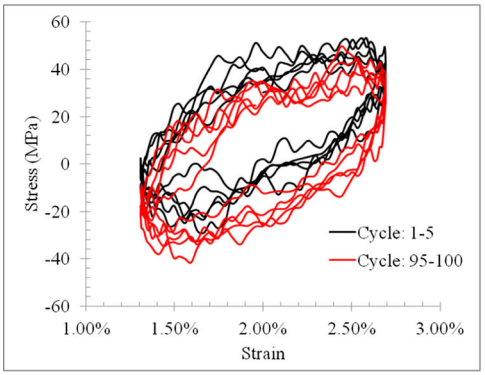

(c) Mean strain: 2%, R-ratio 0.48

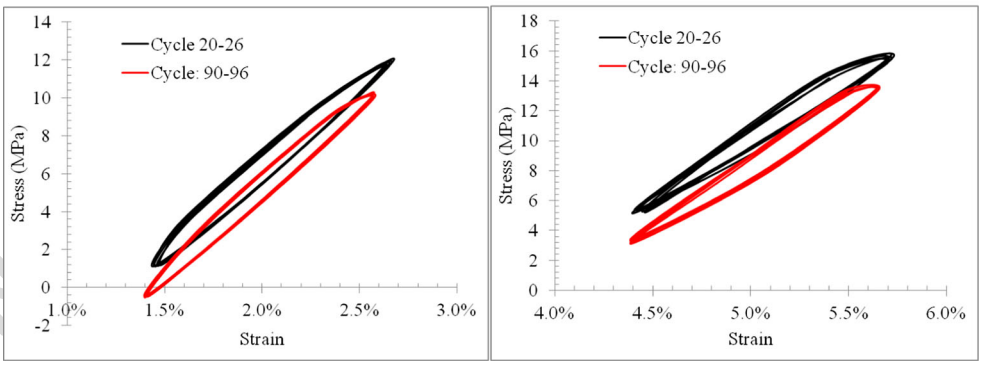

Mean strain 2%, R-ratio 0.48 Mean strain 5%, R-ratio 0.75

(d) Experimental laboratory results

Fig. 8 Stress–strain responses from the MD simulations (**a**–**c**) and experiments (**d**)

The total potential energy is a combination of the potential energies related to the interactions within a chain (bond stretch, bond angle, and dihedral angle torsion) and interchain interactions (van der Waals). The negative values of the total potential energy as shown in Fig. 9 indicate that the van der Waals potential gives the most significant contribution to the system. The negative values of van der Waals potential represent the attractive forces that bind the chains of polymers together in the system which makes them solid.

In the first few cycles the total potential energy normalized to the equilibrium energy is less than one. This indicates that the total potential energy becomes less negative or smaller than the total potential energy after the equilibrium steps because of the application of the initial strain, as illustrated in Fig. 10. The attractive forces become weaker during the initial loading and the stiffness is reduced. In Fig. 10, force is shown as the derivation of a typical Lennard-Jones potential energy and stiffness is the derivation of the force. These are the well-known molecular effects when applying a load to a structural material.

After a few fatigue cycles, a different behaviour is observed. The normalized potential energy increases. The attractive forces binding the polymer chains together increase beyond the original equilibrium level. As a result, the stiffness of

t3.1 **Table 3** Cyclic modulus of the MD simulations and experiments with various mean strains

t3.2 Mean strain	Simulation (GPa)		Experiments (GPa)	
t3.3	Cycles: 1–2	Cycles: 99–100	Cycles: 20–26	Cycles: 90–96
t3.4 2 %, R=0.48	3.01	3.42	0.88	0.91
t3.5 5 %, R=0.75	2.64	2.88	0.82	0.84
t3.6 10 %, R=0.87	2.30	3.13	*NA*	*NA*

NA not available

the system also increases in the simulations. A stiffness increase was also observed in the laboratory experiments as shown in Tables 2 and 3. An increase in the stiffness causes the mean stress reduction as shown in Fig. 7.

Figure 11 presents the evolution of the individual potential energy (bond stretch, angle, dihedral, and van der Waals) vs. the number of cycles in the simulation for a typical case: a mean strain of 2 % and an R-ratio of 0.48. The mean van der Waals potential energy changes by about 3,000 kcal/mol during the first 100 fatigue cycles within 100,000 fs. The van der Waals energy changes much more than the other three energies. The mean dihedral energy changes about half as much (1,500 kcal/mol). The mean bond and angle energies change by less than 500 kcal/mol. The energy change per cycle represented by the amplitude remains fairly constant for all cycles. It is about 750 kcal/mol for the van der Waals energy and 250 kcal/mol for the three other energies.

Movement between chains, as described by the van der Waals energy, dominates the total potential energy evolution behaviour as shown in Fig. 11. Most of the change happens in the first 60,000 fs or 60 cycles. But the last 10 cycles show a further drop of energy indicating more rearrangement between the polymer chains.

Polymer chain rotations, as presented by the dihedral potential energy, are less important. The dihedral potential evolution shows a decreasing trend with increasing number of cycles (time). The decrease of energy indicates a growing number of dihedral bonds in the 'trans' state, which is the lowest energy state. The other two energies show less variation in magnitudes because they are stronger forces binding the monomers in the polymer chains. The small changes indicate that the bond distances increase slightly and the bond angles get closer to equilibrium.

This shows that the movement of the polymer chains against each other such that the van der Waals forces increase is the most important deformation process. The chains also align themselves a bit in the load directions by rotations, which should also help the chains to get closer to each other.

Figure 12 presents the effect of R-ratio and mean strain on the normalized potential energy evolution, $V(t)/V_{eq}$. Increasing the R-ratio from 0.48 to 0.67 increases the mean of the normalized potential energy. However, increasing the R-ratio from 0.67 to 0.9 does not change significantly the mean of the normalized potential energy, but it significantly reduces the amplitude. Reduction of the amplitude is expected since there is a reduction in loading amplitude. Increasing the mean strain from 2 to 10 % does not change significantly the mean of the normalized potential energy. Note that the higher mean strain reduces the normalized potential energy at the first few cycles because of the higher initial strain. Therefore, a higher mean strain reduces the initial stiffness of the system as shown in the simulations and is similar to the experiments as shown in Table 3.

Another way to look at changes to the molecular structure is to look at the characteristics of bond lengths and angles.

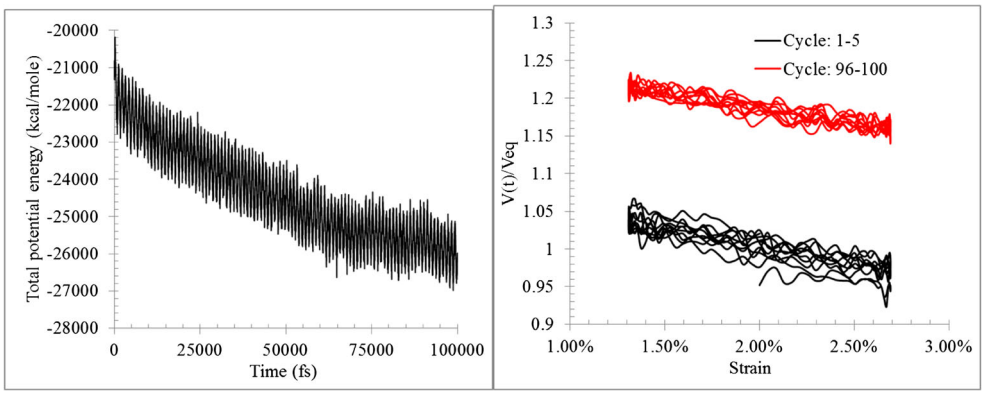

Fig. 9 Potential energy evolution of the MD simulation (mean strain 2 % and R-ratio 0.48)

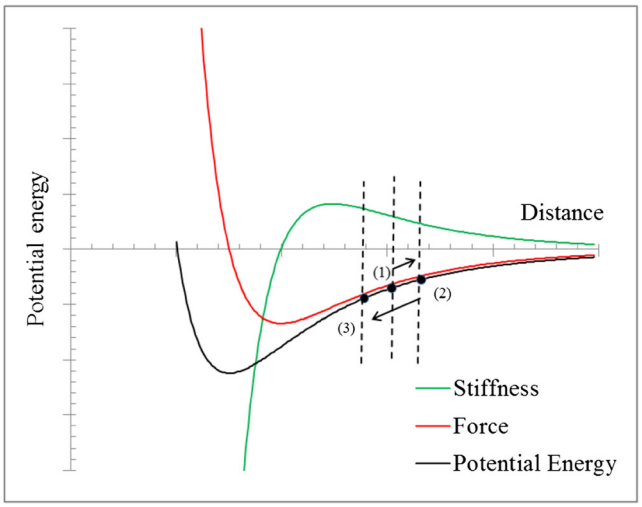

Fig. 10 Illustration of the total potential energy evolution: (1) Energy after equilibrium step. (2) Energy after initial loading. (3) Energy after applying sinusoidal loading

Using the Kolmogorov-Smirnov normality test [37] with α= 1 %, it is found that all bond distance and bond angle distributions, before any loading and after fatigue loading, are normal distributions. The effect of R-ratio and mean strain on the variation of bond distances and bond angles at the end of the simulations are not significant, as shown in Table 4. However, a difference between the original (before any loads were applied) dihedral angle distribution and after fatigue can be seen in Table 4. The percentage of trans state and mean of trans state angle shows a minor increase after fatigue loading. This would have been expected from the potential energy reduction for dihedral angles described earlier. The number of the lower energy trans angles has increased slightly. The dihedral angle distribution function changes were also minor for polycarbonate compressed with a strain of 0.68 at a temperature of 135 K as indicated by experimental NMR data [38].

Percentage of trans state of each chain before and after fatigue simulation is shown in Table 5. The percentage of trans state of each chain increases slightly after fatigue loading is applied. Mechanical work from fatigue loading results in the change of some gauche states to trans states of each chain and the related decrease in dihedral energy. The torsional movement of dihedral angles, as gauche states rotate to trans states, is also related to the non-bonded energy (i.e. van der Waals) between polymer chains. By the torsional movement, the chains align themselves in the load directions, which should also help the chains to get closer to each other and reduce the non-bonded energy.

The radius of gyration was calculated as the root mean square distance between its centre of mass position of the chain and each monomer position in that chain:

$$R_g^2 = \frac{1}{M}\sum m_i(r_i - r_{cm})^2 \quad (7)$$

where M is the total mass of the chain and r_{cm} is the center-of-mass position of the chain [39]. The x, y, and z components of the radius of the gyration tensor can be determined using the same formula.

This property is an indication of the level of compaction or how folded or unfolded the chains are. The radius of gyration along the x axis (the loading direction) is increasing at the end of simulation while those of the other two axes (y and z) are decreasing. Table 6 shows the radius of gyration of each chain along the x axis (the loading direction) before and after fatigue loading is applied. It can be seen that the radius of gyration of each chain increases slightly after fatigue loading is applied. On average, the radius of gyration along the x axis (the loading direction) is increasing by 3.7 %, 3.9 %, and 4.0 % for the R-ratios of 0.48, 0.67, and 0.9, respectively. This agrees with SANS (small-angle neutron scattering) data which indicate that the radius of gyration of linear polyethylene film increases along the stretching direction (using a draw ratio of 5.3) at room temperature [40]. In this study, strains were much lower, as more typically

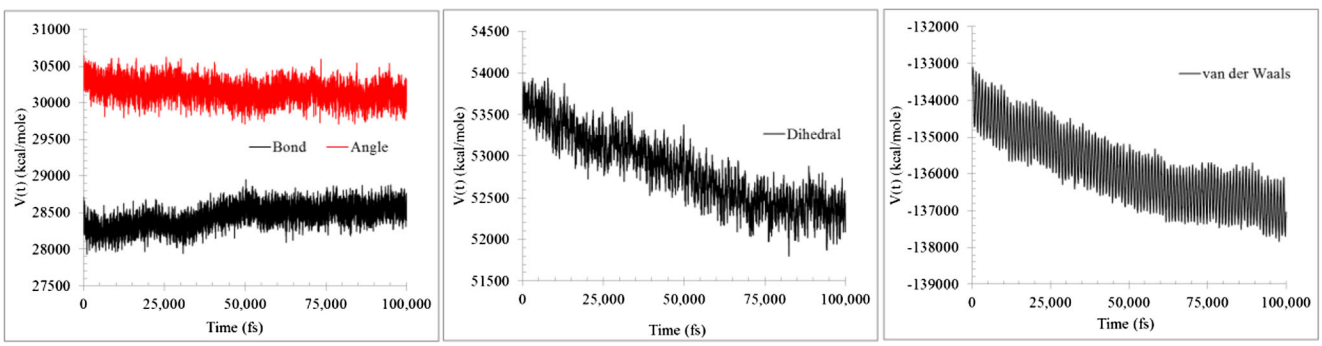

Fig. 11 Individual potential energy evolutions of the MD simulation (mean strain 2 % and R-ratio 0.48)

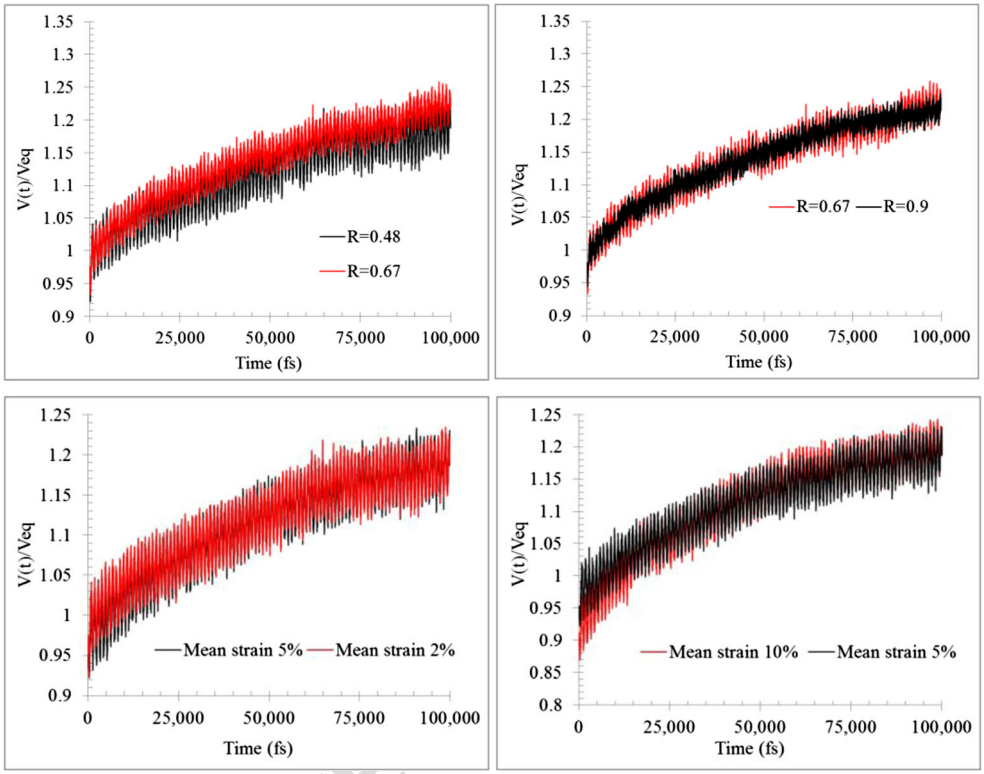

Fig. 12 Effect of R-ratio and mean strain on the potential energy evolution

applied in commercial applications. For this reason, only minor changes in the chain configuration are found. This result indicates that fatigue loading under low strain causes the polymer chains to unfold slightly along the loading axis and become firmly packed along the other two directions. This movement contributes to the reduction of van der Waals energy and increases the stiffness observed in the experiments.

Table 4 Statistical data of polymer geometries at the beginning and the end of the fatigue simulation

	Original	Mean strain = 2 %			Mean strain	
		R=0.48	*R*=0.67	*R*=0.9	5 %	10 %
Bond distance						
Mean	1.53	1.53	1.53	1.53	1.53	1.53
Standard Deviation	0.03	0.03	0.03	0.03	0.03	0.03
Bond Angle						
Mean	109.30	109.29	109.29	109.29	109.31	109.33
Standard Deviation	4.07	4.03	4.04	4.03	4.06	4.07
Dihedral angle: Trans state						
Mean	169.47	180.11	180.03	180.05	180.03	180.00
Standard Deviation	8.74	13.39	13.28	13.24	13.40	13.44
Percentage	64.92 %	66.13 %	66.19 %	66.14 %	66.30 %	66.48 %
Dihedral angle: Gauche + state						
Mean	66.87	66.72	66.84	66.56	66.73	66.66
Standard Deviation	12.99	13.19	12.99	12.91	13.15	12.97
Percentage	17.68 %	16.97 %	17.03 %	17.18 %	16.87 %	16.74 %
Dihedral angle: Gauche – state						
Mean	−66.90	−66.88	−66.72	−66.64	−66.78	−66.68
Standard Deviation	13.37	13.14	13.00	12.81	13.19	13.00
Percentage	17.40 %	16.90 %	16.78 %	16.67 %	16.84 %	16.79 %

t5.1 **Table 5** Trans state percentage of each chain before and after loading

t5.2		Percentage of trans state			
t5.3	Chain	Original	R=0.48	R=0.67	R=0.9
t5.4	1	64.88 %	65.95 %	66.20 %	66.92 %
t5.5	2	64.70 %	65.95 %	66.72 %	66.01 %
t5.6	3	65.77 %	66.70 %	66.00 %	66.36 %
t5.7	4	64.78 %	66.68 %	66.18 %	65.97 %
t5.8	5	65.57 %	65.92 %	66.33 %	65.46 %
t5.9	6	64.55 %	65.86 %	65.73 %	65.58 %
t5.10	7	65.29 %	65.59 %	65.99 %	66.43 %
t5.11	8	64.18 %	66.12 %	66.06 %	65.96 %
t5.12	9	64.59 %	66.13 %	65.79 %	66.23 %
t5.13	10	64.86 %	66.54 %	66.88 %	66.35 %

Conclusions

The molecular dynamics (MD) simulation approach has been applied to study fatigue of amorphous polyethylene on the molecular and global level. The effect of R-ratio and mean strain on strain-controlled fatigue behaviour of amorphous polyethylene was investigated.

The MD simulations are able to produce qualitatively similar behaviour as observed experimentally in the laboratory, for instance, mean stress relaxation, hysteresis loops in the stress–strain curve, and change in the cyclic modulus. Increasing R-ratio increases mean stress and cyclic modulus, while increasing the mean strain increases mean stress, but decreases the cyclic modulus. These trends were properly reproduced even though simulations were done at much higher strain rates and on polymers with low molecular weight being completely amorphous. These limitations should be removed in the future when computer power increases, allowing use of more accurate models. The simulations also showed that cyclic fatigue increases the effect of stress relaxation slightly, showing an interaction between cyclic fatigue and creep.

On the molecular level, an increasing number of fatigue cycles causes mainly a change of the van der Waals potential energy. This change is caused by movements between polymer chains, creating more aligned dihedral configurations. This increases the stiffness of the polymer and, therefore, the reduction of the mean stress. But the main effect creating a higher modulus is due to the chains moving closer together. Bond angles and distances change only slightly for fatigue under low strain. This was demonstrated by small changes in bond and angle potential energies.

t6.1 **Table 6** Radius of gyration of each chain along the loading direction before and after loading

t6.2		Radius of gyration (Å)			
t6.3	Chain	Original	R=0.48	R=0.67	R=0.9
t6.4	1	1,567.0	1,645.8	1,637.6	1,629.5
t6.5	2	2,427.2	2,517.3	2,510.1	2,544.3
t6.6	3	1,711.2	1,763.7	1,769.6	1,753.0
t6.7	4	1,136.0	1,143.2	1,176.8	1,177.6
t6.8	5	2,127.7	2,187.7	2,222.7	2,226.4
t6.9	6	832.5	874.5	861.7	870.5
t6.10	7	1,449.3	1,512.0	1,513.5	1,514.1
t6.11	8	1,731.1	1,800.7	1,796.0	1,803.1
t6.12	9	2,244.2	2,330.9	2,323.7	2,316.5
t6.13	10	642.3	675.5	676.9	668.7

Acknowledgments This research was financed by the Norwegian University of Science and Technology (NTNU). Computational resources at NTNU were partially provided by NOTUR, http://www.notur.no. This support is gratefully acknowledged.

References

1. Lesser AJ (1995) Changes in mechanical behavior during fatigue of semicrystalline thermoplastics. J Appl Polym Sci 58(5):869–879
2. Khelif R, Chateauneuf A et al (2008) Statistical analysis of HDPE fatigue lifetime. Meccanica 43(6):567–576
3. Wyzgoski MG, Novak GE (2005) Predicting fatigue S-N (stress-number of cycles to fail) behavior of reinforced plastics using fracture mechanics theory. J Mater Sci 40(2):295–308
4. Crawshaw J, Windle AH (2003) Multiscale modelling in polymer science. Fibre Diffract Rev 11:52–67
5. Kremer K, Müller-Plathe F (2002) Multiscale simulation in polymer science. Mol Simul 28(8):729–750
6. Baeurle SA, Usami T, Gusev AA (2006) A new multiscale modeling approach for the prediction of mechanical properties of polymer-based nanomaterials. Polymer 47(26):8604–8617
7. Baschnagel J, Binder K, Doruker P, Gusev AA, Hahn O, Kremer K, Mattice WL, Müller-Plathe F, Murat M, Paul W, Santos S, Suter UW, Tries W (2000) Bridging the Gap between atomistic and coarse-grained models of polymers: status and perspectives. Viscoelast, Atomistic Model, Stat Chem, Adv Polym Sci 152:41–156
8. Meyer RW, Pruitt LA (2001) The effect of cyclic true strain on the morphology, structure, and relaxation behavior of ultra high molecular weight polyethylene. Polymer 42(12):5293–5306
9. Seguela R (2005) Critical review of the molecular topology of semicrystalline polymers: the origin and assessment of intercrystalline tie molecules and chain entanglements. J Polym Sci B Polym Phys 43(14):1729–1748
10. Brown D, Clarke JHR (1991) Molecular dynamics simulation of an amorphous polymer under tension. 1. Phenomenology. Macromolecules 24(8):2075–2082
11. Yang L, Srolovitz DJ, Yee AF (1997) Extended ensemble molecular dynamics method for constant strain rate uniaxial deformation of polymer systems. J Chem Phys 107(11):4396–4407
12. Capaldi FM, Boyce MC, Rutledge GC (2004) Molecular response of a glassy polymer to active deformation. Polymer 45(4):1391–1399
13. Sahputra IH, Echtermeyer AT (2013) Effect of temperature and strain rate on the deformation of amorphous polyethylene: comparison

between molecular dynamics simulations and experimental results. Model Simul Mater Sci Eng 21:065016
14. Hossain D, Tschopp MA, Ward DK, Bouvard JL, Wang P, Horstemeyer MF (2010) Molecular dynamics simulations of deformation mechanisms of amorphous polyethylene. Polymer 51(25): 6071–6083
15. Yashiro K (2010) Molecular dynamics simulation of polyethylene under cyclic loading: effect of loading condition and chain length. Int J Mech Sci 52(2):136
16. Li C, Jaramillo E, Strachan A (2013) Molecular dynamics simulations on cyclic deformation of an epoxy thermoset. Polymer 54(2): 881–890
17. Chen P, Wong SC (2011) Strain-controlled fatigue life and modeling of conduit polymers. J Mater Sci 46(6):1902–1912
18. Tao G, Xia Z (2007) Mean stress/strain effect on fatigue behavior of an epoxy resin. Int J Fatigue 29(12):2180–2190
19. Avanzini A (2011) Effect of cyclic strain on the mechanical behavior of virgin ultra-high molecular weight polyethylene. J Mech Behav Biomed Mater 4(7):1242–1256
20. Liang T, Tokunaga K, Yamashita A, Takahara A, Kajiyama T (1996) Relationships between nonlinear dynamic viscoelasticity and fatigue behaviors of glassy polymer under various fatigue test conditions. Polym Bull 36(4):477–482
21. Hizoum K, Rémond Y, Patlazhan S (2011) Coupling of nanocavitation with cyclic deformation behavior of high-density polyethylene below the yield point. J Eng Mater Technol 133(3): 030901–030901
22. Mayo SL, Olafson BD, Goddard WW III (1990) DREIDING: a generic force field for molecular simulations. J Phys Chem 94(26): 8897–8909
23. Plimpton S (1995) Fast parallel algorithms for short-range molecular dynamics. J Comput Phys 117(1):1–19
24. Shinoda W, Shiga M et al (2004) Rapid estimation of elastic constants by molecular dynamics simulation under constant stress. Phys Rev B 69(13):134103
25. Martyna GJ, Tobias DJ et al (1994) Constant pressure molecular dynamics algorithms. J Chem Phys 101(5):4177–4189
26. Parrinello M, Rahman A (1981) Polymorphic transitions in single crystals: a new molecular dynamics method. J Appl Phys 52(12): 7182–7190
27. Mark ET, José A et al (2006) A Liouville-operator derived measure-preserving integrator for molecular dynamics simulations in the isothermal–isobaric ensemble. J Phys A Math Gen 39(19):5629
28. Fakirov S, Krasteva B (2000) On the glass transition temperature of polyethylene as revealed by microhardness measurements. J Macromol Sci Part B: Phys 39(2):297–301
29. Mahajan DK, Basu S (2010) On the simulation of uniaxial, compressive behaviour of amorphous, glassy polymers with molecular dynamics. Int J Appl Mech 02(03):515–541
30. Nakajima A, Hamada F, Hayashi S (1967) Unperturbed chain dimensions of polyethylene in theta solvents. J Polym Sci Part C: Polym Symp 15(1):285–294
31. Branch MA, Coleman TF, Li Y (1999) A subspace, interior, and conjugate gradient method for large-scale bound-constrained minimization problems. SIAM J Sci Comput 21(1):1–23
32. Byrd RH, Schnabel RB, Shultz GA (1988) Approximate solution of the trust region problem by minimization over Two-dimensional subspaces. Math Program 40:247–263
33. Zhou Y, Lu X, Zhou Z, Brown N (1996) The relative influences of molecular structure on brittle fracture by fatigue and under constant load in polyethylenes. Polym Eng Sci 36(16): 2101–2107
34. Sauer J, Richardson G (1980) Fatigue of polymers. Int J Fract 16(6): 499–532
35. Runt J, Jacq M (1989) Effect of crystalline morphology on fatigue crack propagation in polyethylene. J Mater Sci 24(4):1421–1428
36. Li X, Hristov HA, Yee AF, Gidley DW (1995) Influence of cyclic fatigue on the mechanical properties of amorphous polycarbonate. Polymer 36(4):759–765
37. D'Agostino RB, Stephens MA (eds) (1986) Goodness-of-Fit Techniques, Marcel Dekker
38. Utz M, Robyr P, Suter UW (2000) Solid-state NMR investigation of the structural consequences of plastic deformation in polycarbonate. 2. Local orientational order. Macromolecules 33(18):6808–6814
39. Gedde UW (1995) Polymer physics. Chapman & Hall
40. Men Y, Riege J, Lindner P, Enderle H-F, Lilge D, Kristen MO, Mihan S, Jiang S (2005) Structural changes and chain radius of gyration in cold-drawn polyethylene after annealing: small- and wide-angle X-ray scattering and small-angle neutron scattering studies. J Phys Chem B 109(35):16650–16657

AUTHOR QUERY

AUTHOR PLEASE ANSWER QUERY.

Q1. Please check that the figure caption is accurate and ammend if necessary.